MITSUBISHI ELECTRIC RESEARCH LABORATORIES
https://www.merl.com

Adaptive Hybrid Prediction-Correction with Trust-Region and Dynamic Line Search for AC/DC Load Flow

Singh, Deepi; Sun, Hongbo; Kawano, Shunsuke; Raghunathan, Arvind; Takaguchi, Yusuke; Luo, Fang

TR2026-067 June 04, 2026

Abstract

Hybrid AC/DC power systems are gaining importance due to the rising penetration of Distributed Energy Resources (DERs) and the widespread deployment of Voltage Source Converters (VSCs). Analyzing power flow in such systems remains challenging due to unbalanced operating conditions, strong nonlinearities, and strict operational limits. This paper presents an Adaptive Hybrid Prediction–Correction algorithm with Trust-Region and Dynamic Line Search (AHPC-TRDLS) for reliable and efficient load flow computation in large-scale hybrid systems. The framework couples a Newton–Raphson- based prediction stage with a Preconditioned Conjugate Gradient (PCG) correction, bounded adaptively by a trust-region radius. A dynamic line search mechanism is incorporated as a fall- back whenever the PCG convergence stalls, ensuring numerical stability. Additional features include adaptive preconditioning, enforcement of voltage and reactive power limits, and the use of symmetrical components for unbalanced system modeling. The algorithm is implemented in MATLAB and evaluated on different hybrid AC/DC test systems of varying scales. Case studies confirm that the proposed approach offers improved convergence, robustness, and scalability under stressed, ill-conditioned, and unbalanced scenarios.

IEEE Transactions on Power Delivery 2026

Mitsubishi Electric Research Laboratories, Inc.
201 Broadway, Cambridge, Massachusetts 02139

Adaptive Hybrid Prediction-Correction with Trust-Region and Dynamic Line Search for AC/DC Load Flow

Deepi Singh, *Student Member, IEEE*, Hongbo Sun, *Senior Member, IEEE*, Shunsuke Kawano, Arvind Raghunathan, *Member, IEEE*,Yusuke Takaguchi, and Fang Luo, *Senior Member, IEEE*

***Abstract*—Hybrid AC/DC power systems are gaining importance due to the rising penetration of Distributed Energy Resources (DERs) and the widespread deployment of Voltage Source Converters (VSCs). Analyzing power flow in such systems remains challenging due to unbalanced operating conditions, strong nonlinearities, and strict operational limits. This paper presents an Adaptive Hybrid Prediction–Correction algorithm with Trust-Region and Dynamic Line Search (AHPC-TRDLS) for reliable and efficient load flow computation in large-scale hybrid systems. The framework couples a Newton–Raphson-based prediction stage with a Preconditioned Conjugate Gradient (PCG) correction, bounded adaptively by a trust-region radius. A dynamic line search mechanism is incorporated as a fall-back whenever the PCG convergence stalls, ensuring numerical stability. Additional features include adaptive preconditioning, enforcement of voltage and reactive power limits, and the use of symmetrical components for unbalanced system modeling. The algorithm is implemented in MATLAB and evaluated on different hybrid AC/DC test systems of varying scales. Case studies confirm that the proposed approach offers improved convergence, robustness, and scalability under stressed, ill-conditioned, and unbalanced scenarios.**

***Index Terms*—AC/DC power systems, prediction-correction, trust-region, dynamic line search.**

I. Introduction

MODERN power systems are undergoing a rapid transformation driven by the large-scale integration of Renewable Energy Sources (RES), the expansion of long-distance bulk power transfer, and the growing need for asynchronous interconnections [1, 2]. Hybrid AC/DC networks, enabled by Voltage Source Converter (VSC)–based High-Voltage Direct Current (HVDC) technology, have emerged as a key component of this transition. VSCs offer bidirectional power transfer, fast and independent control of active and reactive power, black-start capability, and compatibility with weak or islanded grids.

In these hybrid systems, steady-state Load Flow (LF) or Power Flow (PF) analysis remains essential for operational planning, stability assessment, and security evaluation. However, PF computation in AC/DC grids is challenging due to: (i) the coexistence of multiple bus types and converter control modes (P–Q, V_{dc}–Q, P–$|V_{ac}|$, droop, etc.); (ii) strong nonlinear coupling between AC and DC subsystems via converter equations; (iii) high variability in R/X ratios across transmission, distribution, and DC feeders; (iv) possible unbalanced three-phase operating conditions; and (v) the need to enforce diverse physical limits such as generator reactive power (Q) limits, converter P/Q capabilities, and DC voltage bounds [3]–[5]. Table I summarizes the various bus types and converter control modes commonly found in hybrid AC/DC PF studies.

TABLE I
Bus and Converter Control Modes of Hybrid AC/DC System

Bus Type	Control Mode	Known Var.	Unknown Var.
AC Slack	–	$\|E_{ac}\|,\ \angle E_{ac}$	$P_{ac},\ Q_{ac}$
AC PQ	–	$P_{ac},\ Q_{ac}$	$\|E_{ac}\|,\ \angle E_{ac}$
AC PV	–	$P_{ac},\ \|E_{ac}\|$	$Q_{ac},\ \angle E_{ac}$
AC-side Converter (IC_{ac})	PQ	$P_{ac},\ Q_{ac}$	$\|E_{ac}\|,\ \angle E_{ac}$
	E_{dc}–Q_{ac}	Q_{ac}	$P_{ac},\ \|E_{ac}\|,\ \angle E_{ac}$
	P_{ac}–$\|E_{ac}\|$	$P_{ac},\ \|E_{ac}\|$	$Q_{ac},\ \angle E_{ac}$
DC-side Converter (IC_{dc})	PQ	P_{dc}	E_{dc}
	E_{dc}–Q_{ac}	E_{dc}	P_{dc}
	P_{dc}–E_{dc}	P_{dc}	E_{dc}
DC PQ	–	P_{dc}	E_{dc}
DC Volt.	–	E_{dc}	P_{dc}

A. Existing PF Solution Approaches

PF algorithms for hybrid AC/DC systems are broadly classified as *sequential* or *unified*. In sequential methods, AC and DC subsystems are solved independently with iterative exchange of converter boundary conditions [6, 7]. They are simple and modular but often suffer from slow or unstable convergence under strong AC–DC coupling, multiple V_{dc}-controlling converters, or poor initialization. Enhancements such as auxiliary states [7] and relaxation factors improve stability but increase computational effort.

Unified formulations integrate AC, DC, and converter models into a single nonlinear system, enabling strong coupling and consistent representation [8, 9]. Key developments include transformer-like two-port VSC models [10], the Flexible Universal Branch Model (FUBM) [11], AC-equivalent DC formulations [12], and droop-aware MTDC extensions [13, 14]. MANA-based approaches [15, 16] extend unified load flow formulations to DC-distributed networks and multiphase microgrids, offering the flexibility to represent ar-

Deepi Singh conducted this work during her internship at Mitsubishi Electric Research Laboratories. (*Corresponding author: Hongbo Sun*)

Deepi Singh and Fang Luo are with the Department of Electrical and Computer Engineering, Stony Brook University, NY, 11790, USA (email: deepi.singh@stonybrook.edu, fang.luo@stonybrook.edu).

Hongbo Sun and Arvind Raghunathan are with Mitsubishi Electric Research Laboratories, Cambridge, MA, 02139, USA (email:hongbosun@merl.com, raghunathan@merl.com).

Shunsuke Kawano and Yusuke Takaguchi are with Advanced Technology R&.D Center, Mitsubishi Electric Corporation, Amagasaki, Japan (email:kawano.shunsuke@dn.mitsubishielectric.co.jp, Takaguchi.Yusuke@ce.mitsubishielectric.co.jp).

bitrary topologies and diverse component models. However, challenges persist with numerical conditioning, scalability, and simplified converter models. Iterative simplifications such as the Improved Unified Iteration Method (IUIM) [17] reduce state dimensionality by nearly 80% compared to UIM and demonstrate real-time feasibility, though at the cost of Q-flow accuracy and large-network scalability. Equivalent-circuit approaches [18] capture converter conduction and switching losses with adaptive step-size control, but require careful tuning and lack multiphase validation.

More generalized formulations [19] extend Jacobians to support multiple V_{dc}-controlling converters and unbalanced operation, although robustness and scalability challenges persist for unbalanced and ill-conditioned systems. Emerging approaches such as Multiphase Element-based (MELF) [20] and holomorphic embedding [21] enhance NR convergence and initialization-independence, respectively, but remain constrained by Q-limit handling and restriction to balanced steady-state scenarios.

Persistent challenges: Despite notable progress, unified PF solvers still face several unresolved issues:

- **Numerical fragility** under ill-conditioned Jacobians, high R/X ratios, and weak-grid conditions [22]–[24].
- **Scalability limitations** caused by dense Jacobian factorization and repeated assembly in large MTDC or multiphase systems [25].
- **Instability in limit enforcement**, where PV↔PQ, VQ↔PQ, generator-Q limits, voltage bounds, and converter P/Q curves trigger oscillatory switching or infeasible updates [11, 19, 26].
- **Convergence degradation in converter-dominated or unbalanced operation**, particularly with multiple V_{dc}-controlling interconnecting converters [14, 19].

B. Contributions of This Work

This paper introduces an Adaptive Hybrid Prediction–Correction with Trust-Region and Dynamic Line-Search (AHPC-TRDLS) algorithm for unified power-flow analysis in hybrid AC/DC networks. The solver builds upon the Multi-Phase Trust-Region Prediction–Correction (MPTR-PC) framework—formulated in this work as a foundational reference—and extends it into a curvature-adaptive, converter-aware, and trust-region-regulated architecture that improves numerical robustness and scalability under nonlinear converter dynamics and heterogeneous-grid operating conditions.

The main contributions are summarized as follows:

- Unified tri-layer solver architecture: Couples predictor–corrector guidance, adaptive trust-region step bounding, and fallback line-search within a single iterative loop, ensuring globalized convergence without switching between solver modes.
- Curvature-adaptive extension of MPTR-PC: Residual-trend monitoring and curvature-based damping to regulate step acceptance; the fallback line-search is activated only when trust-region ratios indicate model unreliability, improving stability over conventional TR–PCG or Newton methods.

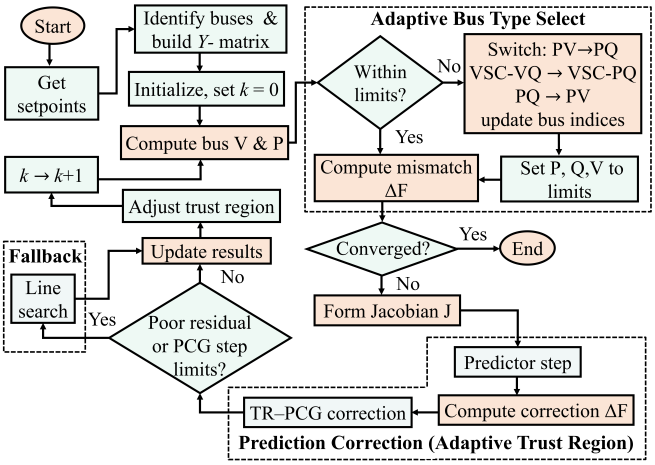

Fig. 1. Flowchart of the proposed AHPC-TRDLS algorithm for unified hybrid AC/DC power flow analysis.

- Converter-aware adaptivity: Synchronizes PV↔PQ and VQ↔PQ transitions and enforces V_{dc}, generator-Q, and converter-power limits coherently within each iteration. The converter model is embedded directly into the unified AC/DC state vector—without auxiliary converter variables—ensuring coherent numerical treatment of AC, DC, and converter constraints within the same loop.
- Sparse and scalable correction: Employs preconditioned conjugate-gradient updates on sparse Jacobians, achieving improved computational growth validated across IEEE-30, IEEE-57–14, EPFL μ-grid, and PEGASE-1354 systems.
- Comprehensive benchmarking across heterogeneous systems: Validated on transmission, distribution, asynchronous hybrid, and large-scale AC/DC systems (IEEE 30, IEEE 57–14, EPFL μ-grid, PEGASE-1354), demonstrating consistent convergence and 3.9×–25× runtime improvement over the MATPOWER–FUBM solver.

By coupling curvature-adaptive step control with converter-coordinated limit enforcement, the AHPC-TRDLS algorithm provides a unified and scalable foundation for reliable hybrid AC/DC power-flow computation.

C. Organization of the Paper

The remainder of this paper is organized as follows. Section II, Section III, and Section IV present the proposed methodology, including an overview of the proposed algorithm, the formulation of power flow equations for hybrid AC/DC networks, and the unified AHPC–TRDLS solution algorithm that integrates prediction–correction, trust-region enforcement, and line search techniques. Section V introduces the case study setup, system models, and simulation conditions. Section VI discusses the numerical results under various operating scenarios, along with scalability and benchmarking results for hybrid AC/DC systems. Sections VII and VIII highlight the potential for real-time and renewable energy integration, followed by a discussion of limitations and future scope. Finally, Section IX concludes the paper and outlines future research directions.

II. Methodology

Overview: The proposed AHPC-TRDLS algorithm enables efficient load flow analysis in hybrid AC/DC grids with multiple VSCs, unbalanced conditions, and operational constraints. As outlined in Fig. 1, the algorithm follows two main steps: prediction using Newton-Raphson (NR) and correction using Preconditioned Conjugate Gradient (PCG) within a trust-region framework. If PCG fails, a dynamic line search ensures convergence. The iterative process continues until voltage and reactive power constraints are satisfied. The key components are:

- Prediction (NR step): Initializes state variables using a three-phase Newton-Raphson method. The Jacobian incorporates AC, DC, and VSC subsystems.
- Correction (PCG with trust-region): Refines the prediction using PCG while constraining step size via a dynamically updated trust radius. Diagonal preconditioning improves numerical stability.
- Fallback (Dynamic line search): If the PCG step fails to achieve sufficient reduction or exhibits stagnation, a backtracking line search is activated to ensure descent and maintain trust-region feasibility in ill-conditioned cases.
- Handling unbalanced systems: Unbalanced three-phase voltages and currents are represented through the Fortescue symmetrical component transformation, which decomposes phase-domain quantities into positive, negative, and zero sequence components. This representation provides a systematic framework for accurately capturing asymmetries with converter interactions, while preserving compatibility with sequence-domain PF formulations.
- Adaptive bus and converter control with constraint enforcement: The algorithm supports adaptive switching of bus types and converter control modes to preserve feasibility under diverse operating conditions. For generator and load buses, PV↔PQ transitions are invoked when voltage or reactive power limits are dynamically violated. VSCs' control mode shifts between PQ and VQ when their operational constraints are exceeded. In all cases, the Jacobian and mismatch formulations are consistently updated to reflect the new classifications, ensuring stable convergence of the load flow even under challenging scenarios, such as variability introduced by renewable generation.
- Scalability and efficiency: Leveraging sparse matrix operations and iterative solvers, the algorithm applies to large-scale hybrid AC/DC networks with multiple DERs and HVDC links.

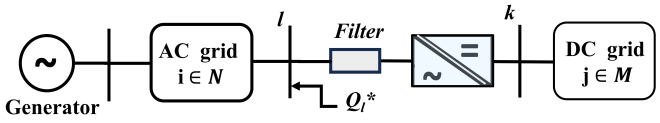

Fig. 2. General diagram of a hybrid AC/DC system [19].

III. PF Equations for Hybrid AC/DC Networks

Consider a hybrid AC/DC network consisting of N AC nodes and M DC nodes, with AC/DC converter buses denoted as $(l,k) \in \Gamma$, where $l \in N$ and $k \in M$ as shown in Fig. 2.

A. AC Network Power Flow Equations

The AC network power flow equations for each type of bus are as follows:

(a) For PQ buses:

$$\Re\left\{ E_i^{\varphi} \sum_{n\in N} Y^{*}_{ac(i,n)}\, E_n^{\varphi *} \right\} = \hat{P}_i^{\varphi}, \quad i \in N_{PQ} \tag{1}$$

$$\Im\left\{ E_i^{\varphi} \sum_{n\in N} Y^{*}_{ac(i,n)}\, E_n^{\varphi *} \right\} = \hat{Q}_i^{\varphi} \quad i \in N_{PQ} \tag{2}$$

(b) For PV buses:

$$\Re\left\{ E_i^{\varphi} \sum_{n\in N} Y^{*}_{ac(i,n)}\, E_n^{\varphi *} \right\} = \hat{P}_i^{\varphi} \quad i \in N_{PV} \tag{3}$$

$$\left(E_i^{\varphi'}\right)^2 + \left(E_i^{\varphi''}\right)^2 = \left(\hat{E}_i^{\varphi}\right)^2 \quad i \in N_{PV} \tag{4}$$

where $\hat{P}_i^{\varphi}$ and $\hat{Q}_i^{\varphi}$ denote the active and reactive power injections at node i and phase $\varphi \in \{a,b,c\}$, respectively. The quantity $\hat{E}_i^{\varphi}$ represents the nodal phase-to-ground voltage phasor. The superscripts $(\cdot)'$, $(\cdot)''$, and $(\cdot)^*$ denote the real part, imaginary part, and complex conjugate, respectively. The matrix Y_{ac} is the AC network admittance matrix. When sequences are referenced, they are formed via the Fortescue transform (Appendix IX-A).

B. DC Network Power Flow Equations

(a) For P-nodes in the DC grid:

$$E_j \sum_{m\in M} Y_{dc(j,m)}\, E_m = \hat{P}_j \quad j \in M_P \tag{5}$$

(b) For V-nodes in the DC grid:

$$E_j = \hat{E}_j \quad j \in M_V \tag{6}$$

where Y_{dc} represents the DC network admittance matrix, and $\hat{P}_j$ and $\hat{E}_j$ denote the prescribed DC power and voltage setpoints, respectively.

C. VSC Modeling

VSCs are the controllable interfaces between AC and DC subsystems and, in Back-to-Back (BTB) configurations, between two AC areas. In steady state, the VSC model determines which variables are regulated, which balances are enforced, how losses are placed, and how unbalance is handled. Accurate modeling is therefore essential for: (i) robust convergence on weak grids (high R/X), (ii) credible results under unbalanced operation, (iii) proper handling of capability and $Q/|E|$ limits via bus–type switching, and (iv) coupling of asynchronous AC areas through a common DC link.

TABLE II
VSC CONTROL MODES

Mode	Constraint 1	Constraint 2	Control Type
1	θ_{sh}	E_{ac}	
2	P_f	Q_{ac}	I
3	P_f	E_{ac}	
4	E_{dc}	Q_{ac}	II
5	E_{dc}	E_{ac}	
6	E_{dc} droop	Q_{ac}	III
7	E_{dc} droop	E_{ac}	

*1) **VSC Operating Modes**:* In steady state, the chosen operating mode fixes which balances are enforced at each converter's AC and DC terminals (Table II). The formulation of the converter power balances adopted here follows the extended VSC model proposed in [19].

(a) E_{dc}–Q_{ac}Mode: Control objectives: (i) regulate the DC-link voltage to $\hat{E}_k$, and (ii) regulate AC reactive power at bus l to $\hat{Q}_l$. Power balance at the interface $(l,k) \in \Gamma_{E_{dc}Q}$ requires

$$\sum_{\varphi\in\{a,b,c\}} P_l^{\varphi} \;+\; P_{\text{loss}(l,k)} \;+\; P_{\text{filter}(l,k)} = P_k \tag{7}$$

$$\sum_{\varphi\in\{a,b,c\}} Q_l^{\varphi} \;-\; Q_{\text{loss}(l,k)} = \hat{Q}_l \tag{8}$$

where subscripts l and k refer to the AC and DC sides, respectively, and $\hat{Q}_l$ is the reactive setpoint. The reactive power loss across the filter is already accounted for in the VSC setpoint $\hat{Q}_l$.

i. Balanced: The power is distributed equally across the three phases:

$$P_l^{\varphi} = \frac{1}{3}P_k, \qquad Q_l^{\varphi} = \frac{1}{3}\hat{Q}_l \tag{9}$$

ii. Unbalanced (Phase-Locked Loop (PLL) aligned to the positive sequence): Only positive-sequence power is injected, as the inner current controllers track the positive-sequence components. The zero-and negative-sequence components are constrained at the terminal [27]:

$$P_l^0 = 0, \quad P_l^+ + P_{\text{loss}(l,k)}^+ + P_{\text{filter}(l,k)}^+ = P_k, \quad P_l^- = 0 \tag{10}$$

$$Q_l^0 = 0, \quad Q_l^+ - Q_{\text{loss}(l,k)}^+ = \hat{Q}_l, \quad Q_l^- = 0 \tag{11}$$

with

$$P_l^+ = \Re\left\{ E_l^+ \sum_{n\in N} Y_{ac(l,n)}^* E_n^{+*} \right\} \tag{12}$$

$$Q_l^+ = \Im\left\{ E_l^+ \sum_{n\in N} Y_{ac(l,n)}^* E_n^{+*} \right\} \tag{13}$$

The DC-side active power is given by

$$P_k^+ = \Re\left\{ \hat{E}_k \sum_{m\in M} Y_{dc(k,m)} E_m \right\} \tag{14}$$

where $\hat{E}_k$ denotes the DC voltage reference. To ensure zero homopolar components, either the voltage E_l^0 or the current I_l^0 must be zero. For a Voltage Source Converter (VSC), E_l^0 is set to zero. Conversely, for a Current Source Converter (CSC), I_l^0 is set to zero. The same constraint applies to the negative-sequence component. Using the positive-sequence components, the DC voltage $\hat{E}_k$ satisfies:

$$\begin{aligned} Y_{dc_{(k,k)}}(\hat{E}_k)^2 + \sum_{\substack{m\in M \\ m\neq k}} Y_{dc(k,m)} E_m \hat{E}_k \\ - \Re\left\{ E_l^+ \sum_{n\in N} Y_{ac(l,n)}^* E_n^{+*} \right\} = 0 \end{aligned} \tag{15}$$

Solving this quadratic equation yields two solutions for $\hat{E}_k$, of which the physically feasible solution is typically close to 1 p.u. [19].

(b) P_{ac}–Q_{ac} Mode: Control objective: impose the scheduled AC active and reactive power at the converter AC bus l (optionally per sequence), while the DC side follows from the power balance, including converter and filter losses.

i. Unbalanced: the zero-sequence voltage is constrained at the terminal ($E_l^0 = 0$). Two practices are supported:

1) Positive-sequence only: set $E_l^- = 0$ and enforce P_l^+ and Q_l^+ as in (16) and (18).
2) Explicit negative-sequence support: enforce both positive- and negative-sequence components:

$$\Re\left\{ E_l^+ \sum_{n\in N} Y_{ac(l,n)}^* E_n^{+*} \right\} - P_{\text{loss}(l,k)}^+ = \hat{P}_l^+ \tag{16}$$

$$\Re\left\{ E_l^- \sum_{n\in N} Y_{ac(l,n)}^* E_n^{-*} \right\} - P_{\text{loss}(l,k)}^- = \hat{P}_l^- \tag{17}$$

$$\Im\left\{ E_l^+ \sum_{n\in N} Y_{ac(l,n)}^* E_n^{+*} \right\} - Q_{\text{loss}(l,k)}^+ = \hat{Q}_l^+ \tag{18}$$

$$\Im\left\{ E_l^- \sum_{n\in N} Y_{ac(l,n)}^* E_n^{-*} \right\} - Q_{\text{loss}(l,k)}^- = \hat{Q}_l^- \tag{19}$$

ii. Balanced: impose $E_l^0 = 0$ and $E_l^- = 0$ and apply the positive-sequence enforcement only (see (16) and (18)).

The associated DC active-power balance (including the converter and filter losses) is

$$\hat{P}_l = \Re\left\{ E_k \sum_{m\in M} Y_{dc(k,m)} E_m \right\} - P_{\text{loss}(l,k)} - P_{\text{filter}(l,k)} \tag{20}$$

Table III summarizes the mapping between converter control modes and the enforced equations under balanced and unbalanced operating conditions.

*2) **VSC Loss Model**:* For steady-state PF studies, the AC/DC interfacing converter is represented by a transformer-like VSC with an RL interface filter and two loss contributions: an AC-side conduction drop and a DC-side switching loss source [19].

(a) Detailed (Transformer-Like) Model: The conduction drop on the AC side is modeled as

$$E_{c(l,k)} = R_{\text{eq}}\big(|I_l|\big)\, I_l \tag{21}$$

TABLE III
CONVERTER OPERATING MODES AND APPLIED CONSTRAINTS

Mode	Balanced case	Unbalanced case
$\boldsymbol{E_{dc}}$–$\boldsymbol{Q_{ac}}$	$E_l^0 = E_l^- = 0$; enforce Q_l^+, E_k	$E_l^0 = E_l^- = 0$; P_l^+, Q_l^+; zero seq. blocked; negative seq. suppressed by control.
$\boldsymbol{P_{ac}}$–$\boldsymbol{Q_{ac}}$	$E_l^0 = E_l^- = 0$; enforce P_l^+, Q_l^+	$E_l^0 = 0$; P_l^+, Q_l^+ enforced, with optional P_l^-, Q_l^-.
$\boldsymbol{P_{ac}}$–$\boldsymbol{\lvert E_{ac}\rvert}$	$E_l^0 = E_l^- = 0$; enforce $P_l^+, \lvert E_l\rvert$	$E_l^0 = 0$; enforce $P_l^+, \lvert E_l^\phi\rvert$; zero seq. fixed by topology.

Note: Losses are embedded as in (23)–(25).

where $R_{\mathrm{eq}}(\cdot)$ is the effective IGBT conduction resistance (possibly current-dependent via data-sheet fits) [19, 28]. The switching loss is modeled as a DC-side current source:

$$I_{\mathrm{sw}(l,k)} = 2\,\frac{T_{\mathrm{ON}} + T_{\mathrm{OFF}} + T_{\mathrm{rr}}}{T_s}\;\frac{1}{N}\;\cot\!\Big(\frac{\pi}{N}\Big)\,|I_l| \tag{22}$$

where T_s is the switching period and $N = f_s/f_{\mathrm{grid}}$ is the ratio of the converter switching frequency to the grid frequency. The parameters T_{ON} and T_{OFF} denote the turn-on and turn-off times of the switches, while T_{rr} represents the diode reverse recovery time during turn-off.

The total converter loss power follows directly as the sum of conduction and switching losses:

$$S_{\mathrm{loss}(l,k)} = E_{c(l,k)} \sum_{n\in N} Y^*_{ac(l,n)} E^*_n + I_{\mathrm{sw}(l,k)} E_k \tag{23}$$

with a purely resistive conduction drop in (21) and steady DC current in (22), S_{loss} is real and $Q_{\mathrm{loss}} = 0$.

(b) Aggregate (Quadratic) Model: At the HVDC station level, losses are often aggregated as

$$P_{\mathrm{loss}(l,k)} = a + b\,|I_l| + c\,|I_l|^2 \tag{24}$$

where a (W) represents no-load and auxiliary losses, b (W/A) captures switching losses, and c (Ω) reflects conduction losses [29]. The benchmarking study employs a quadratic loss model with $a = 0.011$, $b = 0.0034$, and $c = 0.011$ p.u., as defined in (24) [19, 30, 31].

(c) Filter Loss: For a series filter impedance $Z_{\mathrm{filter}(l)}$, the active filter loss is

$$P_{\mathrm{filter}(l,k)} = \Re\left\{ Z_{\mathrm{filter}(l)} \left| \sum_{n\in\mathcal{N}} Y_{ac(l,n)}\,\bar{E}_n \right|^2 \right\} \tag{25}$$

(d) Integration of Losses in PF: The terms P_{loss} and P_{filter} enter the active-power equations (7), (10), and (20), while Q_{loss} is subtracted in the reactive-power equations (8) and (11) (and appears on the right-hand side of (18)–(19) accordingly). If the controller embeds the reactive effect of the filter in $\hat{Q}_l$, no explicit Q_{filter} term is added.

D. BTB Interconnection and Multi–Frequency Grids

A BTB station consists of two VSCs sharing a common DC link and interfacing two AC areas that may differ in frequency, phase, and grid strength (Figs. 3 and 4). Each converter synchronizes locally via a PLL and operates under its assigned control mode (e.g., one in E_{dc}–Q_{ac} mode to regulate the DC voltage $\hat{E}_k$, and the other in P_{ac}–Q_{ac} mode to schedule active power transfer and local reactive power support). In the PF formulation, this appears as (i) two converter equation blocks (as above) and (ii) shared DC node balances coupling their active powers (including both converters' losses), thereby decoupling AC frequencies while maintaining the scheduled transfer.

IV. UNIFIED SOLUTION USING AHPC-TRDLS

To solve the power flow equations for the hybrid AC/DC network, we apply the Newton-Raphson method with integrated prediction-correction, trust-region, and line search methods.

1. Mismatch Vector Calculation: Calculate power and voltage mismatches at all AC/DC buses and VSC-controlled nodes (Table II). The mismatch vector is defined as

$$\Delta F = \begin{bmatrix} \Delta P_{ac} & \Delta Q_{ac} & \Delta E_{dc} & \Delta P^+_{ac} & \Delta Q^+_{ac} \\ \Delta E^{0'}_{ac} & \Delta E^{-'}_{ac} & \Delta E^{0''}_{ac} & \Delta E^{-''}_{ac} & \Delta P_{dc} \end{bmatrix} \tag{26}$$

where ΔP_{ac} and ΔQ_{ac} are active and reactive power mismatches at AC buses; ΔE_{dc} and ΔP_{dc} denote DC voltage and power mismatches; ΔP^+_{ac} and ΔQ^+_{ac} correspond to positive-sequence power mismatches; and $\Delta E^{0'}_{ac}, \Delta E^{-'}_{ac}, \Delta E^{0''}_{ac}, \Delta E^{-''}_{ac}$ represent zero- and negative-sequence voltage mismatches.

2. Jacobian Matrix Construction: The Jacobian submatrices account for AC-bus power mismatches and VSC-related voltage and power mismatches in the hybrid AC/DC network. The Jacobian matrix J is formulated using partial derivatives as;

$$J \;=\; \frac{\Delta F}{\Delta X} \;=\; \begin{bmatrix} J_{(\cdot),E'} & J_{(\cdot),E''} & J_{(\cdot),E_{dc}} \end{bmatrix} \tag{27}$$

where the row blocks follow the ordering of ΔF and the column blocks follow the ordering of ΔX. Explicit expressions for all Jacobian blocks are provided in Appendix IX-B.

The vector of unknown variables is defined as

$$\Delta X^T = \begin{bmatrix} \Delta E' & \Delta E'' & \Delta E_{dc} \end{bmatrix}$$

3. Predictor Step: The predictor step provides an initial estimate of the system state update by solving the system

$$\Delta X_{\text{pred}} = J^{-1} \Delta F \tag{28}$$

The voltage updates after the predictor step are computed as

$$E'_{\text{pred}} = E' + \delta\,\Delta X', \tag{29}$$

$$E''_{\text{pred}} = E'' + \delta\,\Delta X'' \tag{30}$$

The step size δ is adjusted based on the mismatch norm as

$$\delta = \begin{cases} \dfrac{\delta}{2}, & \text{if } \|\Delta F\| > \|\Delta F_{\text{old}}\| \\ \min(2\delta, \delta_{\max}), & \text{otherwise} \end{cases} \tag{31}$$

TABLE IV
SOLVER PARAMETERS AND ADAPTIVE RULES FOR AHPC-TRDLS

Parameter	Initial Value / Range	Adaptive Update Rule
δ	$\delta \in [0,1]$, $\delta_{\max} = 1.0$	$\delta \to \delta/2$ if $\|\Delta F\| > \|\Delta F_{\text{old}}\|$; otherwise $\delta \to \min(2\delta, \delta_{\max})$ [Eq. (31)]
R_{trust}	Bal.: 0.0–0.8 Unbal.: 0.25 (well-cond.), 0.40 (ill-cond.) Asym.: 0.70 Rand.: 0.15–2.0	$R_{\text{trust}} \to \min(2R_{\text{trust}}, R_{\text{trust}}^{\max})$ if $\rho > \eta$; otherwise $R_{\text{trust}} \to R_{\text{trust}}/2$, with $R_{\text{trust}}^{\max} = 1$ [Eq. (42), (51)]
η	0.15 (weak/ill-cond.); 0.20 (stable)	Fixed per study; tightened if acceptance is permissive [Eq. (51)]
ϵ	10^{-6}	Applied when $\kappa_J = \text{cond}(J^\top J) > \tau$ [Eq. (36)]
τ	10^8	If $\kappa_J > \tau$: set $M^{-1} = \text{diag}\big(1/\left(\text{diag}(J^\top J) + \epsilon\right)\big)$; else $\epsilon = 0$ [Eq. (36)]
τ_{trend}	Bal.: 1.0–1.5; Unbal.: 1.3; Asym.: 1.2; Rand.: 1.2	Trigger Armijo backtracking if $\|r_i\|/\|r_0\| > \tau_{\text{trend}}$ [Eq. (44)]
β	$\beta_0 = 1.0$	Armijo backtracking: $\beta \to \tau_\beta \beta$, $0 < \tau_\beta < 1$ [Eq. (47)]
$k_{\max}$	100	Stop if $\|\Delta F_{\text{combined}}\| < 10^{-8}$ or $k = k_{\max}$ [Eq. (52)]

Note: R_{trust} is case dependent; smaller values may be used for balanced systems. For randomization studies, $\delta^{\text{int}} \in [0.90,\ 0.95]$; otherwise,1.

where $\delta \in [0,1]$ is the adaptive step size, $\|\Delta F\|$ denotes the current mismatch norm, $\|\Delta F_{\text{old}}\|$ is the mismatch norm from the previous iteration, and $\delta_{\max}$ is the upper bound on the step size.

4. Correction with Preconditioned Conjugate Gradient and Trust-Region constraint: The correction step solves the trust-region subproblem using Preconditioned Conjugate Gradient (PCG):

$$J\Delta X_{\text{corr}} = -\Delta F_{\text{pred}} \tag{32}$$

where ΔF_{pred} is the mismatch vector after the prediction state. The search direction is iteratively determined using the following steps.

(a) Compute the initial residual:

$$r_0 = J^T \Delta F_{\text{pred}} - J^T (J\Delta X_{\text{corr}}) \tag{33}$$

(b) Apply the preconditioner:

$$z_0 = M^{-1} r_0 \tag{34}$$

where M^{-1} is the preconditioner matrix. Adaptive Preconditioning Based on Jacobian Condition Number

$$\kappa_J = \text{cond}(J^T J) \tag{35}$$

where κ_J represents the condition number of the Jacobian matrix. To improve numerical stability, the inverse of the preconditioner matrix is computed as

$$M^{-1} = \begin{cases} \text{diag}\left(\dfrac{1}{\text{diag}(J^T J) + \epsilon}\right), & \text{if } \kappa_J > \tau, \\ \text{diag}\left(\dfrac{1}{\text{diag}(J^T J)}\right), & \text{otherwise} \end{cases} \tag{36}$$

where M^{-1} is the preconditioner used to improve the conditioning of the system, J is the Jacobian matrix, ϵ (10^{-6}) is a small regularization factor to prevent division by near-zero values, and τ is a predefined threshold (10^8) to determine when regularization is needed.

(c) Set the initial search direction:

$$p_0 = z_0 \tag{37}$$

(d) For each iteration k, update the search direction and correction step:

$$Ap_i = J^T (J p_i), \tag{38}$$

$$\alpha_i = \frac{r_i^T z_i}{p_i^T A p_i}, \tag{39}$$

$$\Delta X_{\text{corr}} = \Delta X_{\text{corr}} + \alpha_i p_i \tag{40}$$

(e) Update the residual::

$$r_{i+1} = r_i - \alpha_i A p_i \tag{41}$$

5. Trust-Region Constraints: The trust-region constraint ensures that the update remains within a bounded region:

$$\|\Delta X_{\text{corr}}\| \le R_{\text{trust}} \tag{42}$$

If the correction step violates the trust-region constraint $R_{\text{trust}} \in [0,1]$, the correction step is scaled back as

$$\Delta X_{\text{corr}} = \Delta X_{\text{corr}} \frac{R_{\text{trust}}}{\|\Delta X_{\text{corr}}\|} \tag{43}$$

6. Line Search: The PCG iteration is monitored using the residual trend, defined as r_i/r_0,

$$\frac{r_i}{r_0} > \tau_{\text{trend}} \tag{44}$$

If this ratio exceeds a predefined threshold or the maximum number of PCG iterations is reached without convergence, a fallback correction is triggered using a line-search strategy to ensure stability and progress. The update is computed as

$$X^{(k+1)} = X^{(k)} + \beta\, \Delta X_{\text{corr}} \tag{45}$$

where the step size β is adjusted based on the Armijo condition:

$$0.5\, \|J\Delta X_{\text{corr}}\|^2 - \Delta F_{\text{pred}}^T \Delta X_{\text{corr}} \le c\, \beta\, \|p\|^2 \tag{46}$$

If the condition is not met, β is updated using backtracking:

$$\beta = \tau_\beta \beta, \quad 0 < \tau_\beta < 1 \tag{47}$$

7. Combination of Prediction and Correction Steps:

$$E' = E'_{\text{pred}} + \delta\, \Delta X'_{\text{corr}}, \tag{48}$$
$$E'' = E''_{\text{pred}} + \delta\, \Delta X''_{\text{corr}}. \tag{49}$$

8. Trust-Region Adaptation: The effectiveness of the correction step is evaluated using the ratio of actual to predicted reduction:

$$\rho = \frac{\|\Delta F_{\text{pred}}\| - \|\Delta F_{\text{combined}}\|}{\|\Delta F_{\text{pred}}\| - \|\Delta F_{\text{pred}} + J\Delta X_{\text{corr}}\|} \tag{50}$$

where $\Delta F_{\text{combined}}$ is the mismatch vector after the correction state. Based on the computed value of ρ, the trust-region radius is updated dynamically as

$$R_{\text{trust}} = \begin{cases} \min(2R_{\text{trust}}, R_{\text{trust}_{\max}}), & \text{if } \rho > \eta \\ R_{\text{trust}}/2, & \text{otherwise} \end{cases} \tag{51}$$

where R_{trust} is the trust-region radius, and the value of η is conditionally selected based on system characteristics, allowing adaptive control of trust-region updates across varying grid conditions (Table IV). If the correction step fails to improve the solution ($\rho \leq \eta$), the step is rejected and the trust-region radius is reduced to ensure better control in subsequent iterations.

9. Convergence Criterion: Convergence is achieved when

$$\|\Delta F_{\text{combined}}\| < 10^{-8} \tag{52}$$

Otherwise, the iteration counter is updated as $k \leftarrow k + 1$ and the process continues.

V. Case Study

Two hybrid AC / DC test systems, a small-scale network, and a large-scale network are used to evaluate the AHPC-TRDLS algorithm. These case studies capture diverse control modes, operational limits, and grid complexities, enabling a comprehensive assessment of the algorithm's robustness and practical applicability.

(a) System-1: This is a small-scale six-bus hybrid AC / DC test system (Fig. 3) that evaluates the performance of the algorithm in managing power flow within a network where DC links facilitate power transfer [32]. It includes two AC zones (AC-1: buses 1–2; AC-2: buses 3–4) connected via a DC link interfaced by two VSCs (buses 5 and 6). AC-1 connects to generator G1, while AC-2 links to generator G2. VSC1 operates in control mode 2 mode and VSC2 in mode 4, allowing controlled power exchange between domains (Table II). Voltage and reactive power constraints are enforced to simulate practical operational scenarios.

(b) System-2: Hybrid AC/DC Network The second system is a large-scale hybrid AC/DC network comprising two non-synchronous AC grids interconnected by two HVDC links (Fig. 4) [33]. It includes a mix of generation and load buses, with VSCs interfacing AC and DC subsystems under PQ and VQ control modes. This setup evaluates the algorithm's scalability and stability under diverse load conditions and operational constraints, including power limits and voltage setpoints. Extra AC and DC nodes are included to ensure one line exists at each end of the VSCs.

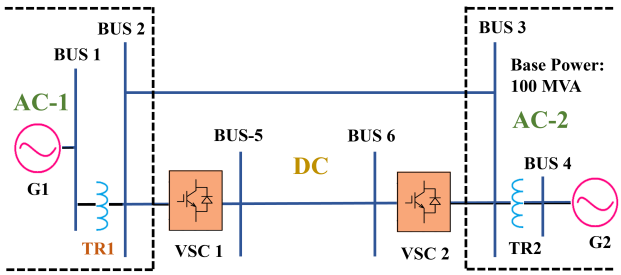

Fig. 3. Schematic diagram of System-1 [32].

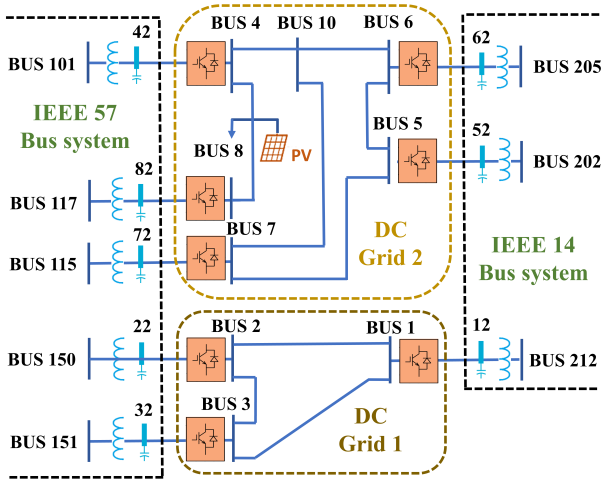

Fig. 4. Schematic diagram of System-2 [33].

(c) Comparison Methodology: AHPC-TRDLS is benchmarked against four methods: standard NR [19], NR with backtracking line search (NR-BLS) [34, 35], $1 + \sqrt{2}$ order NR(a refined NR method designed for improved convergence) [23], and Multi-Phase Trust-Region Prediction-Correction (MPTR-PC) (which integrates trust-region strategies with prediction-correction). Each is evaluated under balanced and unbalanced conditions, examining convergence speed, stability, and computational efficiency under grid stress and limit violations. All methods are tested for tolerance value less than 10^{-8} and a maximum number of iterations of 100.

(d) Implementation Details and parameter selection: The AHPC-TRDLS algorithm is implemented in MATLAB R2024a. Simulations are run on an Intel Core i7-12800HX (32 GB RAM, Windows 11). Key solver parameters are summarized in Table IV. The selected values satisfy the convergence and stability requirements of trust–region and line–search methods [36], while ensuring robustness under nonlinear AC/DC coupling and converter–control interactions [37, 38]. Convergence of these methods typically relies on regularity assumptions such as: the power–mismatch function is

TABLE V
SYSTEM-1 UNDER BALANCED AND UNBALANCED CONDITIONS

Type of System	Balanced		Unbalanced	
Method	**Iter.**	**Time (s)**	**Iter.**	**Time (s)**
NR	11	0.2108	11	0.199
NR-BLS	12	0.2008	12	0.2016
$1+\sqrt{2}$ **order NR**	46	0.2687	46	0.2573
MPTR-PC	12	0.2246	12	0.2117
AHPC-TRDLS	9	0.2050	9	0.2182

TABLE VI
SYSTEM-2 UNDER BALANCED AND UNBALANCED CONDITIONS

Type of System	Balanced		Unbalanced	
Method	**Iter.**	**Time (s)**	**Iter.**	**Time (s)**
NR	16	1.7584	9	1.18
NR-BLS	94	9.4816	96	12.7806
$1+\sqrt{2}$ **order NR**	46	5.5814	44	5.3217
MPTR-PC	16	2.1990	8	1.2214
AHPC-TRDLS	11	1.3719	7	1.2082

continuously differentiable, the Jacobian exhibits local Lipschitz continuity, and each accepted step yields a bounded residual reduction [36]–[38]. In AHPC–TRDLS, the numerical scheme is designed to respect these conditions through: (i) trust–region acceptance governed by the actual–to–predicted reduction ratio ρ, (ii) damping of PCG search directions when residuals rise during nonlinear events such as PV/PQ or VSC–mode switching, and (iii) activation of Armijo backtracking only when PCG no longer provides a reliable descent direction.

The acceptance threshold η and the radius–update rule in Eq. (51) follow the classical ratio test [36]. The initial trust–region radius R_{trust} is chosen according to grid conditioning (balanced, weak, or asymmetrical) to prevent divergence or repeated step rejections [37], and is subsequently updated only via the reduction ratio. The residual–trend tolerance in Eq. (44) serves as a nonmonotone safeguard that delays the line search until the model's predictive accuracy degrades. When $\|\mathbf{r}_i\|/\|\mathbf{r}_0\|$ exceeds its limit, the Armijo backtracking in Eqs. (45), (46), and (47) guarantees sufficient decrease and preserves global convergence [36]. All parameters remain fixed within each operating category, ensuring that performance comparisons reflect intrinsic algorithmic behaviour.

VI. RESULTS AND DISCUSSION

A. Balanced and Unbalanced System Performance

Table V summarizes the performance of various algorithms for System-1 under both balanced and symmetrical unbalanced conditions, reporting the number of iterations and execution time. The power demand for bus 4 and bus 5 has increased to 20 and 10 MW. The unbalanced case includes a 2% voltage deviation and a 5% power mismatch in phases B and C, introducing asymmetry to test the methods under uneven operating conditions.

All methods successfully converge, affirming the relatively small and well-conditioned nature of System-1. The proposed AHPC-TRDLS algorithm requires 9 iterations in both scenarios and achieves low execution time, highlighting its computational efficiency. In contrast, the $1+\sqrt{2}$ NR method converges in 46 iterations, significantly increasing computational effort without notable runtime improvement. Classical NR, NR-BLS, and MPTR-PC methods perform reasonably, requiring 11–12 iterations with runtimes comparable to AHPC-TRDLS.

Table VI compares the algorithms on System-2. The advantages of AHPC-TRDLS become increasingly evident here. While the standard NR method converges in 16 and 9 iterations under balanced and unbalanced conditions, its execution time increases due to system size. The NR method with NR-BLS exhibits slower convergence, requiring 96 iterations and 12.78 seconds under unbalanced conditions.

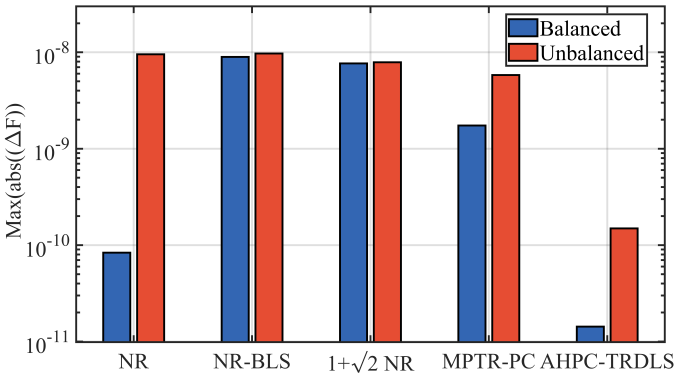

Fig. 5. Maximum mismatch for System-2 under different methods.

On the other hand, AHPC-TRDLS consistently converges in 7–11 iterations with a runtime under 1.4 seconds, demonstrating strong scalability. MPTR-PC also performs well, converging in fewer iterations than conventional methods, though at a slightly higher runtime. These results validate the robustness and computational advantage of AHPC-TRDLS compared to conventional and enhanced Newton-based techniques, particularly for large-scale hybrid AC/DC systems.

The convergence performance of various methods was assessed by comparing the maximum absolute mismatch, $\max|\Delta F|$ for System-2, as shown in Fig. 5. At the same time, the classical NR method demonstrates consistent convergence and is widely recognized for its simplicity and computational efficiency; its sensitivity to asymmetry results in moderately higher residuals. In contrast, the proposed AHPC-TRDLS algorithm consistently achieves superior numerical accuracy across all scenarios, yielding significantly lower mismatch values and demonstrating enhanced robustness under unbalanced and ill-conditioned network conditions.

B. Assessment under Asymmetrical Unbalanced Conditions

To evaluate the resilience of each algorithm under unbalanced operating conditions, System-2 was tested with an intentional 5% increase in voltage magnitude and power injection for Phase C. At the same time, Phases A and B remained at nominal values. This emulates realistic asymmetries found in distribution networks. Under this 5% perturbation, only AHPC-TRDLS and MPTR-PC converged successfully, completing 9 iterations (1.31 s) and 11 iterations (5.16 s), respectively. In contrast, NR, NR with Backtracking Line Search, and $1+\sqrt{2}$ order NR failed to converge at 5%.

TABLE VII
PERFORMANCE WITH LARGE DIFFERENCES IN PARAMETERS (SYSTEM-1)

Type of System	Balanced		Unbalanced	
Method	**Iter.**	**Time (s)**	**Iter.**	**Time (s)**
NR	NC	-	NC	-
NR-BLS	44	0.3014	44	0.2789
$1+\sqrt{2}$ order NR	45	0.2674	45	0.3074
MPTR-PC	47	0.3291	47	0.2971
AHPC-TRDLS	33	0.3161	36	0.2965

Note: NC denotes Not Converged.

However, these methods did achieve convergence under milder imbalances: NR converged at 3% asymmetry in 10 iterations (1.57 s), NR-BLS at 2% in 97 iterations (10.17 s), and $1+\sqrt{2}$ NR at 1% in 43 iterations (5.08 s). These results demonstrate that while classical methods degrade rapidly with asymmetry, AHPC-TRDLS and MPTR-PC maintain robust and efficient convergence across a broader range of operating conditions.

C. Performance Under Large Parameter Variations and Operational Stress

Table VII presents the performance of various algorithms in System-1 under conditions where line parameters—conductance (G) and susceptance (B)—differ significantly. Specifically, the system admittance matrix was modified by increasing the conductance (G) by a factor of 10 and decreasing the susceptance (B) by a factor of 10, creating a challenging numerical environment with high resistance-to-reactance ratios.

Under these conditions, the classical NR method fails to converge for balanced and unbalanced cases, underscoring its sensitivity to ill-conditioning. In contrast, all advanced techniques successfully converge, albeit with varying efficiency. The proposed AHPC-TRDLS algorithm outperforms others by achieving convergence in 33 and 36 iterations for the balanced and unbalanced cases, respectively, while keeping execution times under 0.32 seconds. The MPTR-PC, NR-BLS, and $1+\sqrt{2}$ methods also maintain reliable convergence.

These results underscore the effectiveness of AHPC-TRDLS in handling ill-conditioned or highly heterogeneous networks, maintaining both speed and convergence stability where traditional methods falter.

D. Voltage and Reactive Power Limit Assessment

Bus voltages and reactive power outputs are maintained within predefined bounds ($V \in [0.9, 1.1]$ p.u., $Q \in [-2, 2]$ p.u.) for system-1 and bounds ($V \in [0.94, 1.06]$ p.u.), Q based on PV buses for system-2. For VSCs, active and reactive power are constrained within operational limits ($P, Q \in [-0.5, 0.5]$ p.u.). When any of these constraints are violated, the algorithm dynamically adjusts the modes—for instance, switching from PV to PQ for the generator bus, PQ to PV for the load bus, or from VQ to PQ for VSC-while updating the corresponding Jacobian and mismatch formulations to maintain numerical consistency.

A significant increase in active power demand at Bus 5 in System-1 causes the VSC operating in VQ mode at Bus 3 to exceed its power limit, reaching $S = -0.5012 - 0.0003j$ p.u.

TABLE VIII
PERFORMANCE COMPARISON UNDER LIMIT VIOLATIONS (SYSTEM-1)

Method	Iter.	Time (s)	Total Transitions
NR	23	0.2974	45
NR-BLS	27	0.2839	52
$1+\sqrt{2}$ order NR	58	0.4340	111
MPTR-PC	22	0.3059	39
AHPC-TRDLS	20	0.2236	39

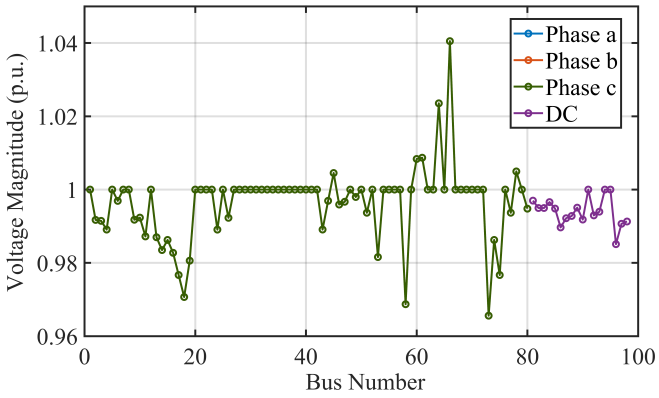

Fig. 6. Per-phase bus voltage profile of System- 2 (balanced, with limits).

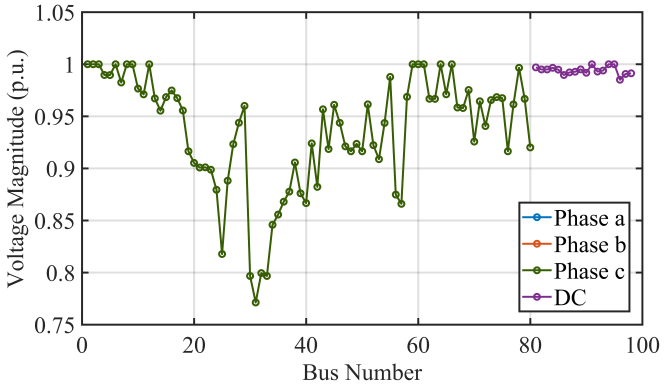

Fig. 7. Per-phase bus voltage profile of System 2 (balanced, without limits).

In response, the algorithm transitions this VSC to PQ control mode and enforces the defined operating limits by clamping the power setpoint to $S = -0.5000 - 0.0003j$ p.u.

The effectiveness of different algorithms under this scenario is summarized in Table VIII, reporting each method's total number of events, iteration count, and computational time.

Figures 6 and 7 illustrate the per-phase bus voltage profiles of System-2 under balanced operating conditions, using the AHPC-TRDLS algorithm with and without limit enforcement, respectively. In Fig. 6, voltage limits on AC and DC buses are strictly enforced during the iteration process, ensuring all bus voltages remain within acceptable operational thresholds. This results in a tightly regulated voltage profile across all phases and buses. Conversely, Fig.7 shows the profile obtained without enforcing these limits.

E. Performance Under Weak Grid Conditions

Tables IX and X summarize the algorithmic performance under weak grid conditions, defined by low X/R ratios (0.5

TABLE IX
WEAK GRID CONDITIONS FOR SYSTEM-1

Type of System	Balanced		Unbalanced	
Method	**Iter.**	**Time (s)**	**Iter.**	**Time (s)**
NR	20	0.2103	20	0.2331
NR-BLS	32	0.2519	32	0.2759
$1+\sqrt{2}$ **order NR**	54	0.2947	54	0.2913
MPTR-PC	17	0.2479	17	0.2231
AHPC-TRDLS	15	0.2559	15	0.2612

TABLE X
WEAK GRID CONDITIONS FOR SYSTEM-2

Type of System	Balanced		Unbalanced	
Method	**Iter.**	**Time (s)**	**Iter.**	**Time (s)**
NR	NC	-	10	1.1837
NR-BLS	91	9.3724	91	9.4897
$1+\sqrt{2}$ **order NR**	48	5.1063	NC	-
MPTR-PC	7	1.1310	7	1.1510
AHPC-TRDLS	13	2.1373	9	1.4643

TABLE XI
UNDER RANDOM PERTURBATION FOR SYSTEM-1

Type of System	Balanced		Unbalanced	
Method	**Iter.**	**Time (s)**	**Iter.**	**Time (s)**
NR	10	0.1927	9	0.181
NR-BLS	12	0.2051	12	0.2165
$1+\sqrt{2}$ **order NR**	41	0.197	44	0.2093
MPTR-PC	9	0.1751	9	0.1847
AHPC-TRDLS	9	0.1816	8	0.1815

TABLE XII
UNDER RANDOM PERTURBATION FOR SYSTEM-2

Type of System	Balanced		Unbalanced	
Method	**Iter.**	**Time (s)**	**Iter.**	**Time (s)**
NR	NC	-	NC	-
NR-BLS	NC	-	NC	-
$1+\sqrt{2}$ **order NR**	43	3.8549	NC	-
MPTR-PC	43	4.4557	47	4.6809
AHPC-TRDLS	10	1.3353	9	1.3036

and 0.95, respectively), which often lead to numerical instability and convergence difficulties. Under weak grid conditions, System-1 exhibits convergence for all methods, though NR, NR-BLS, and $1+\sqrt{2}$ order NR require up to 54 iterations. Despite this, their execution times remain under 0.30 seconds. AHPC-TRDLS achieves convergence in just 15 iterations with a comparable runtime of 0.26 seconds, offering faster convergence without compromising speed.

For System 2, NR fails to converge under balanced conditions and shows limited success for the unbalanced case. NR-BLS and $1+\sqrt{2}$ NR require more than 91 and 48 iterations, respectively, with execution times exceeding 5–9 s. MPTR-PC attains the fastest convergence under both balanced and unbalanced conditions, completing in seven iterations with runtimes of 1.13 s and 1.15 s, respectively. AHPC-TRDLS also performs robustly, converging in 13 and 9 iterations (2.14 s and 1.46 s) while maintaining numerical stability across a broader initialization and grid-strength range.

Robustness Assessment: At $X/R = 0.95$, MPTR–PC exhibits high sensitivity to the initial trust–region radius, achieving convergence primarily near $R_{\text{trust, initial}} \approx 0.2$, whereas AHPC–TRDLS converges over a broader range of $R_{\text{trust, initial}} \in [0.1,\ 0.8]$ with the best runtimes at $R_{\text{trust, initial}} \approx 0.2$–$0.3$. For X/R variations between 0.7 and 1.0, the proposed algorithm maintained monotonic convergence and stable residual decay, whereas MPTR–PC failed to converge for $X/R < 0.8$. This robustness assessment highlights the reduced dependence of AHPC–TRDLS on initialization parameters and its improved adaptability under weak–grid conditions.

F. Performance with Random Perturbation

The performance of System-1 and System-2 under balanced and unbalanced conditions, with random perturbations introduced in the G and B matrices, is summarized in Table XI and Table XII. In System-1, all methods successfully converge. While the conventional NR method achieves convergence in fewer iterations (9–10), the proposed AHPC-TRDLS and MPTR-PC algorithms outperform others by converging within 8–9 iterations and demonstrating the lowest execution times. The $1+\sqrt{2}$ order NR method, though convergent, requires over 41 iterations, indicating reduced efficiency under stochastic variations.

In contrast, System-2 exhibits greater sensitivity to random perturbations. Both the classical NR and NR-BLS methods fail to converge under balanced and unbalanced scenarios. The $1+\sqrt{2}$ NR method only converges in the balanced case, while the MPTR-PC algorithm achieves convergence across both conditions but with relatively high iteration counts (43–47) and longer runtimes (above 4.4 s). The proposed AHPC-TRDLS algorithm remains the most robust, converging within 9–10 iterations and maintaining execution times nearly three times faster than its counterparts, emphasizing its resilience to initialization uncertainty and stochastic disturbances.

G. Scalability and Benchmarking on Hybrid AC/DC Systems

The scalability of the proposed AHPC–TRDLS algorithm is benchmarked against the open-source MATPOWER–FUBM solver [11, 32], which implements a single-phase AC/DC load flow using the Flexible Universal Branch Model. Four representative hybrid AC/DC systems are evaluated under identical initialization (flat start) and convergence tolerance (10^{-8}): (i) the IEEE 30-bus grid with 3- and 5-node MTDC networks [11], (ii) the asynchronous IEEE 57–14 hybrid network [33], (iii) the EPFL hybrid microgrid [19], and (iv) the modified 1354-bus PEGASE transmission grid integrating both a point-to-point HVDC link and a 3-node MTDC subsystem [11]. Table XIII lists the number of iteration counts and computational times for both solvers.

The number of states for the proposed AHPC–TRDLS method and the FUBM formulation are (41 vs. 60), (81 vs. 109), (174 vs. 200), and (2724 vs. 2490) for the EPFL μ-grid, IEEE 30-bus, IEEE 57–14, and PEGASE systems, respectively. The proposed solver achieves runtime reductions of 3.9×–25.3× across all systems while matching or reducing iteration counts. For PEGASE, the FUBM model shows fewer states because it employs a polar coordinate representation,

requiring one variable per PV node, whereas AHPC–TRDLS uses a rectangular formulation with two voltage components per PV node. Conversely, in smaller systems, the FUBM model introduces additional converter-related variables per interface, increasing its Jacobian order and computation time.

A log–log regression of runtime versus state dimension shows that AHPC–TRDLS follows the expected scaling behavior of sparse trust-region PCG iterations, where per-iteration cost grows approximately with the number of nonzero Jacobian entries [39]. For additional benchmarking, a nonlinear interior-point formulation was implemented in YALMIP. For the IEEE 57–14 hybrid system, AHPC–TRDLS converges in 0.075 s compared with 2.12 s for the interior-point solver, and in the PEGASE–1354 case in 2.22 s versus 48.67 s. The contrast highlights the efficiency of the sparse trust-region PCG framework over dense interior-point NLP formulations, especially as problem size increases.

TABLE XIII
BENCHMARKING AGAINST MATPOWER-FUBM

Test System	**FUBM-based**		**Proposed**		**Speedup**
Parameter	**Iter.**	**Time (s)**	**Iter.**	**Time (s)**	**(FUBM/Prop.)**
IEEE 30 Bus	5	0.22719	4	0.011898	19.1
IEEE 57–14 Bus	5	0.26346	5	0.020389	12.9
EPFL μ-grid	11	0.24606	4	0.0097194	25.3
PEGASE	7	7.5535	6	1.9537	3.87

VII. Practical Scope and Integration

The present study has focused on the algorithmic development and offline validation of the AHPC–TRDLS solver. However, several of its characteristics make it well-suited for future integration into energy management systems and real-time simulation platforms. The solver supports the considered converter modes—E_{dc}–Q_{ac}, P_{ac}–Q_{ac}, and P_{ac}–$|E_{ac}|$—by activating only the relevant residuals at the PCC and DC nodes, allowing scheduled transfers across asynchronous or multi-frequency AC grids.

Unbalanced conditions are handled in the sequence domain. PLLs and controllers track the positive sequence by default ($E^0 = E^- = 0$ in E_{dc}–Q_{ac}), while P_{ac}–Q_{ac} mode can enforce both positive and negative sequences setpoints. The framework can also be extended to address renewable uncertainty through adaptive node typing (PV$\leftrightarrow$PQ switching on $Q/|E|$ limits) and converter (P, Q) capability checks with curtailment, thereby providing a pathway to Energy Management System (EMS)-level control. From a practical standpoint, the solver's sparse Jacobian structure, iterative solution with trust-region safeguards, and line-search corrections together ensure scalability and robustness. These features make the algorithm compatible with the computational requirements of real-time execution and EMS applications, positioning it as a strong candidate for future deployment in operational platforms and hardware-in-the-loop studies.

VIII. Limitation and Future Work

Limitations: The proposed method incurs a higher per-iteration computational effort in small systems due to the trust-region and PCG-based correction step. The current validation is restricted to static power-flow scenarios, and dynamic or time-domain interactions have not yet been included. In addition, the present formulation assumes an ideal PLL with positive-sequence synchronization; extensions to non-ideal PLL behavior under unbalance and harmonic distortion are planned.

Future Work: Ongoing development includes coupling the solver with real-time EMS platforms and dynamic/EMT co-simulation environments, incorporating stochastic uncertainty arising from renewable generation and load variations, and conducting broader validation across different converter vendors, modeling platforms, and hybrid AC/DC systems.

IX. Conclusion

This paper has presented the AHPC–TRDLS algorithm for solving power–flow equations in hybrid AC/DC networks. The method integrates Newton–Raphson–based prediction with a preconditioned conjugate–gradient correction inside a trust–region framework, supported by a dynamic line–search fallback. This hybrid formulation balances global convergence control and computational efficiency, improving numerical stability in converter–dominated systems with nonlinear control interactions and operational constraints.

The proposed solver has been validated on a wide range of hybrid networks, including a custom 6–bus test system, the composite IEEE 57–14 asynchronous grid, the experimentally verified EPFL hybrid microgrid, and the large–scale PEGASE 1354–bus transmission system. Across these diverse cases—spanning balanced, unbalanced, and weak–grid conditions—AHPC–TRDLS achieved consistent and stable convergence. While the algorithm occasionally incurs a modest runtime increase under strongly ill–conditioned configurations (e.g., compared with MPTR–PC in System 2's balanced weak grid), this trade–off stems from the additional trust–region and line–search safeguards that guarantee global convergence and prevent divergence in nonlinear regimes.

Comparative benchmarking against the open–source MATPOWER–FUBM platform further confirms the solver's scalability, demonstrating quasi–linear growth with network size and speedups of up to $25\times$ in the EPFL hybrid microgrid and $3.9\times$ in the PEGASE 1354–bus system. These results indicate that AHPC–TRDLS provides a balanced combination of robustness, adaptability, and computational efficiency, suitable for the analysis of modern hybrid AC/DC grids. Future work will extend the framework to dynamic and real–time studies to further bridge numerical reliability and industrial–scale applicability.

APPENDIX

A. Fortescue Transform

Let $\alpha = e^{j2\pi/3}$. The Fortescue transform is defined as

$$T_{\mathrm{sc}} = \tfrac{1}{3}\begin{bmatrix} 1 & 1 & 1 \\ 1 & \alpha & \alpha^2 \\ 1 & \alpha^2 & \alpha \end{bmatrix},$$

which maps phase quantities to sequence components, i.e., $E^{0,+,-} = T_{\mathrm{sc}} E^{a,b,c}$ and $I^{0,+,-} = T_{\mathrm{sc}} I^{a,b,c}$, with $I = Y_{ac} E$.

B. Full Jacobian (Block Form)

$$X = \begin{bmatrix} E' & E'' & E_{dc} \end{bmatrix}^T$$

$$F = \begin{bmatrix} P_{ac}\ Q_{ac}\ E_{dc}\ P_{ac}^{+}\ Q_{ac}^{+}\ E_{ac}^{0'}\ E_{ac}^{-'}\ E_{ac}^{0''}\ E_{ac}^{-''}\ P_{dc} \end{bmatrix}^T$$

$$J = \frac{\Delta F}{\Delta X} = \begin{bmatrix} \frac{\partial F_1}{\partial X} & \frac{\partial F_2}{\partial X} & \cdots & \frac{\partial F_{10}}{\partial X} \end{bmatrix}^T$$

REFERENCES

[1] E. Unamuno and J. A. Barrena, "Hybrid ac/dc microgrids—part i: Review and classification of topologies," *Renewable and Sustainable Energy Reviews*, vol. 52, pp. 1251–1259, 2015.

[2] B. Muruganantham, R. Gnanadass, and N. P. Padhy, "Challenges with renewable energy sources and storage in practical distribution systems," *Renewable and Sustainable Energy Reviews*, vol. 73, pp. 125–134, 2017.

[3] K. Gnanambal, N. Marimuthu, and C. Babulal, "Three-phase power flow analysis in sequence component frame using hybrid particle swarm optimization," *Applied Soft Computing*, vol. 11, no. 2, pp. 1727–1734, 2011.

[4] E. E. Pompodakis, G. C. Kryonidis, C. Demoulias, and M. C. Alexiadis, "A generic power flow algorithm for unbalanced islanded hybrid ac/dc microgrids," *IEEE Transactions on Power Systems*, vol. 36, no. 2, pp. 1107–1120, 2021.

[5] L. Mackay, R. Guarnotta, A. Dimou, G. Morales-España, L. Ramirez-Elizondo, and P. Bauer, "Optimal power flow for unbalanced bipolar dc distribution grids," *IEEE Access*, vol. 6, pp. 5199–5207, 2018.

[6] T. Smed, G. Andersson, G. Sheble, and L. Grigsby, "A new approach to ac/dc power flow," *IEEE Transactions on Power Systems*, vol. 6, no. 3, pp. 1238–1244, 1991.

[7] C. Liu, B. Zhang, Y. Hou, F. F. Wu, and Y. Liu, "An improved approach for ac-dc power flow calculation with multi-infeed dc systems," *IEEE Transactions on Power Systems*, vol. 26, no. 2, pp. 862–869, 2011.

[8] X.-P. Zhang, "Multiterminal voltage-sourced converter-based hvdc models for power flow analysis," *IEEE Transactions on Power Systems*, vol. 19, no. 4, pp. 1877–1884, 2004.

[9] M. Baradar, M. Ghandhari, and D. Van Hertem, "The modeling multi-terminal vsc-hvdc in power flow calculation using unified methodology," in *2011 2nd IEEE PES international conference and exhibition on innovative smart grid technologies*, pp. 1–6, IEEE, 2011.

[10] E. Acha, B. Kazemtabrizi, and L. M. Castro, "A new vsc-hvdc model for power flows using the newton-raphson method," *IEEE Transactions on Power Systems*, vol. 28, no. 3, pp. 2602–2612, 2013.

[11] A. Alvarez-Bustos, *Flexible universal branch model for steady state operational analysis and optimisation of hybrid ac/dc grids*. PhD thesis, Durham University, 2021.

[12] M. M. Rezvani and S. Mehraeen, "Unified ac-dc load flow via an alternate ac-equivalent circuit," *IEEE Transactions on Industry Applications*, vol. 57, no. 6, pp. 5626–5635, 2021.

[13] E. Aprilia, K. Meng, M. Al Hosani, H. H. Zeineldin, and Z. Y. Dong, "Unified power flow algorithm for standalone ac/dc hybrid microgrids," *IEEE Transactions on smart grid*, vol. 10, no. 1, pp. 639–649, 2019.

[14] Q. Nguyen, G. Todeschini, and S. Santoso, "Power flow in a multi-frequency hvac and hvdc system: Formulation, solution, and validation," *IEEE Transactions on Power Systems*, vol. 34, no. 4, pp. 2487–2497, 2019.

[15] Z. Javid, U. Karaagac, and I. Kocar, "Mana formulation based load flow solution for dc distribution networks," *IEEE Transactions on Circuits and Systems II: Express Briefs*, vol. 70, no. 7, pp. 2590–2594, 2023.

[16] N. Rashidirad, J. Mahseredjian, I. Kocar, and U. Karaagac, "Unified mana-based load-flow for multi-frequency hybrid ac/dc multi-microgrids," *Electric Power Systems Research*, vol. 220, p. 109313, 2023.

[17] X. Dong, H. Wang, C. Zhang, W. Yu, R. Yang, L. Xiao, W. Liao, and C. Luo, "The power flow algorithm for ac/dc microgrids based on improved unified iteration method," *Frontiers in Energy Research*, vol. 12, p. 1376714, 2024.

[18] S. Peng, N. Xie, and C. Wang, "A self-adaptive power flow analysis methodology for ac/dc hybrid system," *IEEE Transactions on Power Delivery*, vol. 38, no. 4, pp. 2261–2273, 2023.

[19] W. Lambrichts and M. Paolone, "General and unified model of the power flow problem in multiterminal ac/dc networks," *IEEE Transactions on Power Systems*, 2024.

[20] S. B. Homayie and B. Venkatesh, "General multi-phase element-based load flow for ac–dc power systems," *IEEE Transactions on Power Delivery*, vol. 39, no. 3, pp. 1634–1646, 2024.

[21] Y. Luo and C. Liu, "A unified power flow calculation for hybrid ac/dc power systems based on holomorphic embedding method incorporating lcc-hvdc," *CSEE Journal of Power and Energy Systems*, pp. 1–11, 2025.

[22] M. Tostado, S. Kamel, and F. Jurado, "Developed newton-raphson based predictor-corrector load flow approach with high convergence rate," *International Journal of Electrical Power & Energy Systems*, vol. 105, pp. 785–792, 2019.

[23] Y. Wei, Q. Li, K.-Z. Liu, P. Wang, Z. Zeng, and X. Wang, "A hybrid algorithm for the load flow analysis of vsc-hvdc systems based on 1+ 2 order newton-raphson and simplified newton," *International Journal of Electrical Power & Energy Systems*, vol. 118, p. 105828, 2020.

[24] M. Karimi, A. Shahriari, M. Aghamohammadi, H. Marzooghi, and V. Terzija, "Application of newton-based load flow methods for determining steady-state condition of well and ill-conditioned power systems: A review," *International Journal of Electrical Power & Energy Systems*, vol. 113, pp. 298–309, 2019.

[25] M. D'orto, S. Sjöblom, L. S. Chien, L. Axner, and J. Gong, "Comparing different approaches for solving large scale power-flow problems with the newton-raphson method," *IEEE Access*, vol. 9, pp. 56604–56615, 2021.

[26] L. Zeng, H.-D. Chiang, L. S. Neves, and L. F. C. Alberto, "On the accuracy of power flow and load margin calculation caused by incorrect logical pv/pq switching: Analytics and improved methods," *International Journal of Electrical Power & Energy Systems*, vol. 147, p. 108905, 2023.

[27] IEEE Power System Relaying and Control Committee (PSRC), Working Group C20, "Impact of voltage source converter (VSC) based HVDC transmission on AC system protection," technical report, IEEE Power System Relaying and Control Committee (PSRC), Piscataway, NJ, USA, 2017. System Protection Subcommittee, Working Group C20.

[28] A. K. Sadigh, V. Dargahi, and K. A. Corzine, "Analytical determination of conduction and switching power losses in flying-capacitor-based active neutral-point-clamped multilevel converter," *IEEE Transactions on Power Electronics*, vol. 31, no. 8, pp. 5473–5494, 2016.

[29] J. Renedo, A. A. Ibrahim, B. Kazemtabrizi, A. Garcia-Cerrada, L. Rouco, Q. Zhao, and J. Garcia-Gonzalez, "A simplified algorithm to solve optimal power flows in hybrid vsc-based ac/dc systems," *International Journal of Electrical Power & Energy Systems*, vol. 110, pp. 781–794, 2019.

[30] J. Beerten, S. Cole, and R. Belmans, "Generalized steady-state vsc mtdc model for sequential ac/dc power flow algorithms," *IEEE Transactions on Power Systems*, vol. 27, no. 2, pp. 821–829, 2012.

[31] R. Wachal, A. Jindal, S. Dennetiere, H. Saad, O. Rui, S. Cole, M. Barnes, L. Zhang, Z. Song, J. Jardini, J. Garcia, F. Mosallat, H. Suriyaarachich, P. Le-Huy, A. Totterdell, L. Zeni, S. Kodsi, D. Tiku, P. Thepparat, and Y. Yang, "Guide for the development of models for hvdc converters in a hvdc grid," 12 2014.

[32] A. Alvarez-Bustos, B. Kazemtabrizi, M. Shahbazi, and E. Acha-Daza, "Universal branch model for the solution of optimal power flows in hybrid ac/dc grids," *International Journal of Electrical Power & Energy Systems*, vol. 126, p. 106543, 2021.

[33] R. Chai, B. Zhang, J. Dou, Z. Hao, and T. Zheng, "Unified power flow algorithm based on the nr method for hybrid ac/dc grids incorporating vscs," *IEEE Transactions on Power Systems*, vol. 31, no. 6, pp. 4310–4318, 2016.

[34] R. Idema, "Newton-krylov methods in power flow and contingency analysis," *Thesis*, 2012.

[35] T. T. Truong, "Backtracking new q-newton's method: a good algorithm for optimization and solving systems of equations," *arXiv preprint arXiv:2209.05378*, 2022.

[36] J. Nocedal and S. J. Wright, *Numerical optimization*. Springer, 2006.

[37] K. Tang, S. Dong, J. Shen, C. Zhu, and Y. Song, "A robust and efficient two-stage algorithm for power flow calculation of large-scale systems," *IEEE Transactions on Power Systems*, vol. 34, no. 6, pp. 5012–5022, 2019.

[38] A. Eajal, M. A. Abdelwahed, E. El-Saadany, and K. Ponnambalam, "A unified approach to the power flow analysis of ac/dc hybrid microgrids," *IEEE Transactions on sustainable energy*, vol. 7, no. 3, pp. 1145–1158, 2016.

[39] P. Häusner, O. Öktem, and J. Sjölund, "Neural incomplete factorization: learning preconditioners for the conjugate gradient method," *arXiv preprint arXiv:2305.16368*, 2023.